Autotrophic production, biomass and species composition at two stations across an upwelling front

Raleigh R. Hood*, Susanne Neuer, Timothy J. Cowles

College of Oceanography, Oregon State University, Corvallis, Oregon 97331, USA

ABSTRACT: In early September 1989 persistent southward winds generated an upwelling region along the Oregon, USA, coast with a front (upwelling front) at its seaward edge. We examine and compare autotrophic production, biomass and species composition in the euphotic zones of 2 stations on either side of this front using a combination of analytical techniques. The upwelling front could be seen in satellite thermal imagery all along the southern Washington and Oregon coasts except where it was obscured by the outflow of the Columbia River. Hydrographic profiles at the seaward station showed a relatively warm and deep surface-mixed layer that was freshened by river water. At the landward station the river's influence was much less, and cold, saline water extended to within 10 m of the surface. Chl *a* concentrations were higher in cold water nearshore, and a deep chl *a* maximum was present offshore. On both sides of the front, production rates were highest above 10 % I_o, but the integrated rate nearshore was higher by a factor of 3, and the energy conversion efficiency (from incident solar energy to fixed chemical) of the euphotic zone at the landward station was more than twice that of the seaward station. Flow cytometer analyses revealed 2 distinct autotrophic groups nearshore based on size (volume) and brightness of red fluorescence. Count and size comparisons with epifluorescence microscope observations show that the larger and brighter peak was caused by cryptomonads; this peak was absent seaward of the front. Volume estimates based on epifluorescence microscope observations reveal that at the productive inshore station *Synechococcus* spp., cryptomonads and small autotrophs (< 10 µm) dominated the phytoplankton biomass, and diatoms were a relatively minor component.

INTRODUCTION

The dynamics of coastal upwelling have been understood since the turn of the century, and its effects on primary production are well known (Barber & Smith 1981). Coastal upwelling circulation overrides both the nutrient limitation of stratified waters, and the light limitation of well-mixed waters. When it occurs nutrients are brought into the euphotic zone by vertical transport, and these conditions are maintained by the stabilized offshore flow in the surface layer. This results in optimal conditions for phytoplankton growth. When upwelling persists the enhanced primary production supports higher production at all trophic levels. Ryther (1969) estimated that 50 % of the world's fish catch comes from coastal upwelling areas which comprise 0.1 % of the ocean's area.

Oregon, USA, coastal waters upwell frequently in the late spring and summer months when winds blow southward along the coast (Huyer 1977). It is an ideal place to study plankton response because the upwelling circulation is relatively simple and often persists over periods of many days (Huyer 1983). Upwelling effects on phytoplankton growth off Oregon have been studied extensively (e.g. Curl & Small 1965, Small & Ramberg 1971, Small et al. 1972, Small & Menzies 1981). These studies have shown that the phytoplankton respond rapidly (hours to days) to changes in the upwelling circulation, and they have documented recurring spatial and temporal patterns in phytoplankton biomass (chl *a*) and primary production that are maintained by the upwelling circulation. However, very little is known about the effect upwelling has on phytoplankton species composition off

---

* Present address: Rosenstiel School of Marine and Atmospheric Science, 4600 Rickenbacher Causeway, University of Miami, Miami, Florida 33149, USA

Oregon. It has been assumed that diatoms are responsible for the high chlorophyll concentrations that develop, but there are no published quantitative taxonomic studies of phytoplankton in Oregon coastal waters. There is only indirect evidence that relatively large cells dominate the phytoplankton biomass under upwelling conditions (Kitchen et al. 1975, 1978).

In this paper we examine and compare the euphotic zones of 2 stations on either side of an upwelling front off the Oregon coast using a combination of analytical techniques. We present satellite AVHRR (Advanced Very High Resolution Radiometer) thermal imagery to show the large scale oceanographic setting of the stations, and we use standard hydrographic measurements to contrast them physically. Then we compare autotrophic production, biomass and species composition at the stations using a combination of flow

cytometer, epifluorescence microscope, and ^{14}C uptake rate measurements. We also calculate and compare euphotic zone integrals of various combinations of the biomass, production rate, and light measurements. Our goal is to provide a detailed comparison of autotrophic production, biomass and species composition at 2 stations in very different physical environments.

METHODS

Our stations (18 and 20 in Fig. 1) were sampled on the last 2 d of a 10 d instrument-testing cruise (August 28 through September 7) on the RV 'Wecoma'. Fortuitous circumstances provided an ideal opportunity for a comparison. Persistent upwelling favorable winds had
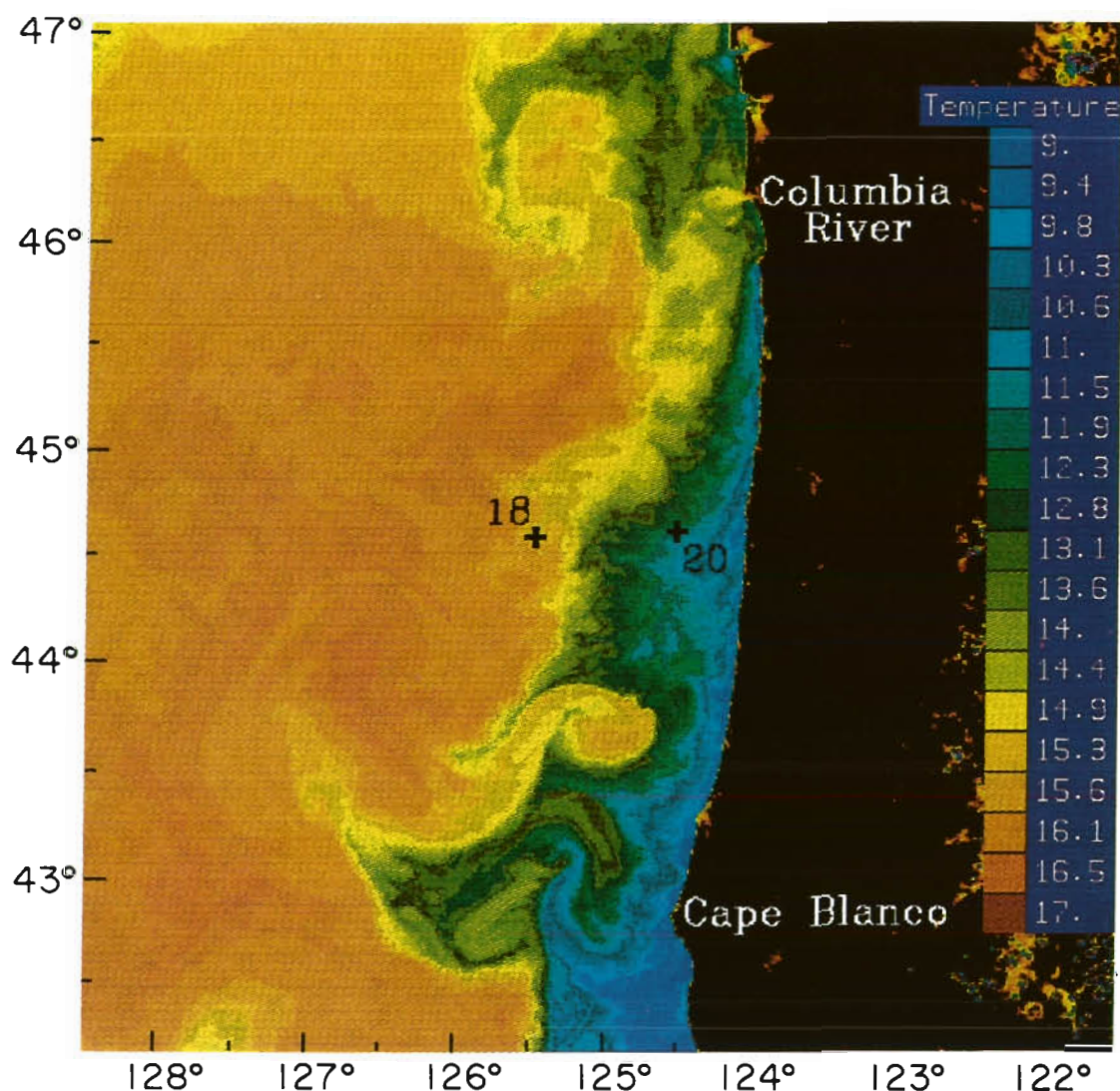

Fig. 1 False-color enhanced satellite AVHRR thermal image of Oregon coastal waters collected on September 6, 1989 with the positions of Stns 18 (seaward) and 20 (landward) superimposed

produced a uniform upwelling region along the coast with a front (hence upwelling front) at its seaward edge and warmer water offshore (see 'Results' and Fig. 1). Although we did not have real-time satellite imagery available to us, we crossed this front heading shoreward near the end of the cruise after sampling on its seaward side (Stn 18) and sampled again on its landward side (Stn 20) the following day.

The satellite AVHRR image was collected at the Scripps Satellite Oceanography Facility. Data were geographically corrected, calibrated to infrared brightness temperature, and linearly false-color enhanced using Miami DSP software. CTD observations were made with a Neil Brown Mark IIIb CTD system. The probe was calibrated for pressure and temperature by the manufacturer, and the conductivity data were calibrated against *in situ* samples. A Seatec fluorometer and transmissometer were attached to the CTD frame. The fluorometer voltage output was not calibrated, and beam transmittance was calculated using the calibration provided by the manufacturer.

A rosette sampler equipped with 5 l Niskin bottles, that were modified and cleaned according to Fitzwater et al. (1982), was used to collect water for the biological analyses. Chl *a* samples were filtered onto Whatman GF/F glass-fiber filters and concentration was determined fluorometrically after 24 h dark extraction in 90 % acetone (Venrick & Hayward 1984). Production rates were measured using a simulated *in situ* version of the ^{14}C incubation method described in Parsons et al. (1984). Samples were incubated from local apparent noon to sunset, and dark bottle activities were subtracted before production rate was calculated. Surface light flux was measured with a continuously recording PAR (photosynthetically available radiation) meter (Biospherical Instruments Inc.), and extinction coefficients (K values) for light attenuation at each station were estimated using a secchi disk.

Flow cytometer measurements were made at sea with a Becton Dickinson FACS Analyzer equipped with a 90 µm aperture. This instrument uses an electrical interference method to estimate relative particle volume (similar to the Coulter Counter), and a low pressure mercury-arc lamp as excitation source. The 436 nm line was used to excite chl *a*, and fluorescence emission was detected at 680 nm. The instrument settings (aperture current, PMT voltages, gain, and volume threshold) were kept constant for all data presented here, and lamp power was monitored continuously. Sample volumes were measured using volume-calibrated sample cuvettes, and data were collected and stored in list mode. Coulter superbright fluorospheres (9.59 µm diameter) were used for signal optimization and volume calibration.

Samples for epifluorescence microscopy were prepared at sea. Subsamples of 30 ml were preserved with glutaraldehyde (3 % final concentration), stained with DAPI (1 mg l^{-1} final concentration), and filtered gently (below 120 mm Hg) onto 0.2 µm black Poretics polycarbonate filters. Each filter was then sandwiched between thin films of immersion oil under a cover slip (as in Booth 1987) and stored frozen (below −15 °C). Slides were counted in the laboratory using a standard epifluorescence microscope configuration (blue excitation: Zeiss filter set 47 77 09, 50 W mercury light). Only counts of autotrophic organisms are presented here (see Table 2); they include phycoerythrin-containing *Synechococcus* spp., cryptomonads, 'unidentified autotrophs < 10 µm' which contains flagellated and coccoid forms that cannot be positively identified under the epifluorescence microscope (e.g. chlorophytes, prymnesiophytes, prasinophytes, chrysophytes and possibly some non-phycoerythrin containing *Synechococcus* spp.), autotrophic cells belonging to the genus *Gymno-Gyrodinium*, and pennate and centric diatoms. Of the *Synechococcus* spp. 100 to 200 cells were counted, of the unidentified autotrophs < 10 µm 20 to 100 cells, of the cryptomonads 10 to 20 cells at the seaward station and 30 to 100 cells at the landward station, and of the larger phototrophic cells, depending upon abundance, 5 to 100 cells were counted in each category. Large cells (> 20 µm diameter) were measured individually to the closest µm, and smaller and more abundant cells were grouped in 2 to 3 µm bins. Cell volumes were calculated from cell dimensions using approximate standard geometric shapes.

RESULTS

Meteorology and satellite imagery

Winds were directed consistently southward (parallel to shore and upwelling favorable) during the cruise and were strongest during a 48 h period prior to sampling when southward velocities consistently exceeded 10 m s^{-1} (RV 'Wecoma' shipboard sail observations). On September 6 and 7, when the seaward station and landward station were sampled (respectively), the winds were lighter (generally less than 10 m s^{-1} southward) and the skies were clear.

Our thermal image (Fig. 1), collected on September 6, revealed a strong upwelling signature (surface water below 12 °C) along the coasts of northern Oregon and southern Washington, except where it was obscured by the warm Columbia River plume. This plume left the coast and flowed southward and seaward on top of the cold, upwelled water, and then its thermal signature disappeared where it extended into warmer water offshore.

The seaward and landward stations were located 120 and 40 km from shore respectively (Fig. 1), on either side of the thermal front between the colder coastal upwelling region nearshore and warmer water offshore. Between the stations the front was 80 km from shore, and the thermal gradient across it was approximately 0.05 °C km^{-1}. The landward station was clearly in the upwelling region along the coast and the seaward station appears to have been in the path of the southward-flowing Columbia River plume offshore.

CTD observations

In Fig. 2 temperature, salinity, and density are plotted down to 5 optical depths ($\simeq$ 1 % I_0) for both stations. The seaward station had a relatively deep (20 m) surface-mixed layer that was warm and less saline, on top of a pronounced pycnocline. At the landward station the mixed layer was relatively shallow (8 m), the surface water was colder and more saline and the pycnocline was less pronounced. At the landward station relatively cold (< 10 °C), saline (> 32.5 psu) water extended up to within 10 m of the surface. The low salinities (below 32 psu) above 20 m at the seaward station confirm that Columbia River water had been mixed in.

The transmissometer and fluorometer traces in Fig. 3 indicate that the phytoplankton were distributed very differently at the 2 stations. At the seaward station there was a pronounced deep fluorescence maximum well below the pycnocline at 3.7 optical depths (2.5 % I_0, 37 m), and it was associated with only a small increase in beam attenuation. At the landward station the fluorescence maximum was just below the pycnocline at an optical depth of about 1.6 (20 % I_0, 9 m), and it was associated with an increase in beam attenuation, but the maxima in fluorescence and beam attenuation were not coincident.

Chlorophyll, production and light

In Fig. 4 the vertical distributions of chl a (extracted), production rate, and light flux (estimated from half-day average surface light flux using secchi-derived extinction coefficients) are plotted against optical depth for both stations. The chlorophyll distribution at the seaward station shows that
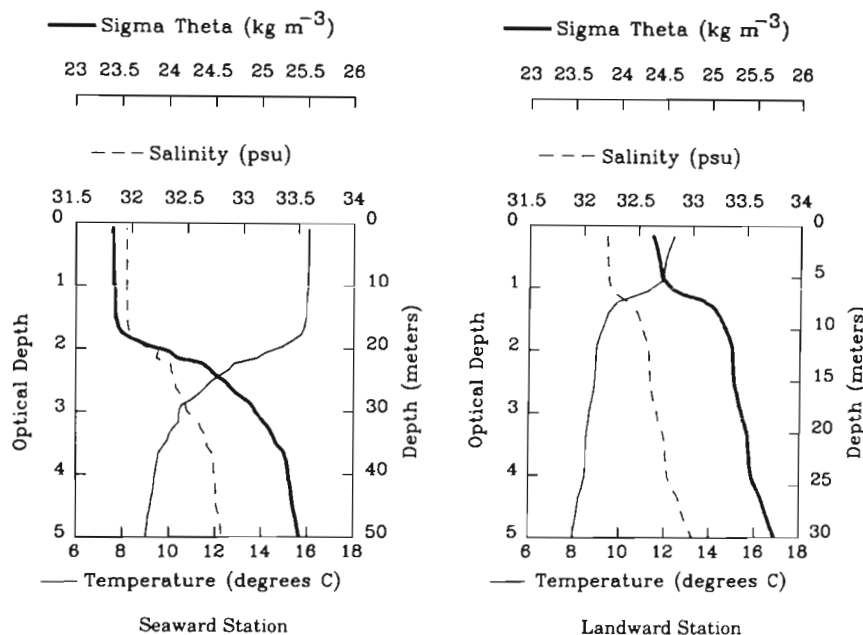

Fig. 2. Vertical profiles of temperature, salinity, and sigma theta scaled to optical depth
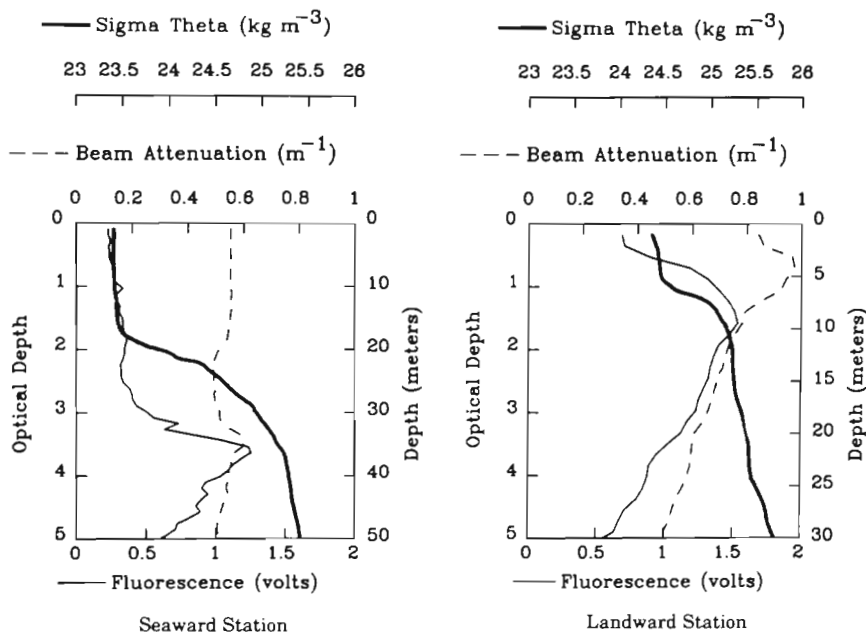

Fig. 3. Vertical profiles of beam attenuation, fluorescence, and sigma theta scaled to optical depth

the increase in fluorescence at depth was associated with an increase in chl *a*, but our discrete samples missed the fluorescence peak. The production rate at the seaward station was highest in the mixed layer above 2 optical depths (10 % I_o, 20 m). Chl *a* concentrations and production rates were substantially higher throughout the euphotic zone (except at 1 % I_o) at the landward station, and both had maxima at 1.2 optical depths (30 % I_o, 7 m). The light (PAR) available in the euphotic zones at the 2 stations was approximately the same.

Integrated chl *a* and production rate, surface light (half-day average I_o (PAR) at the productivity incubators), extinction coefficients (secchi-estimated), and various combinations of these values are compared in Table 1. The integrated chl *a* concentration was nearly twice as high at the landward station, but this difference partly reflects the fact that our discrete samples missed the fluorescence (chl) maximum offshore (using the fluorescence profile in Fig. 3 and a chl/fluorescence ratio of 0.63 we estimate the chl *a* concentration at the fluorescence maximum at the seaward station to have been 0.77 mg m^{-3}, which increases the integrated concentration there by about 18 %). The extinction coefficient was about twice as large nearshore, and even though average light available at the surface was about the same at the 2 stations, the integrated production rate was almost 3 times as high nearshore (missing the deep chl maximum at the seaward station probably did not have a large effect the integrated production rate. Using an interpolated assimilation number of 0.623 mg C (mg chl *a*)$^{-1}$ h^{-1} and the previously estimated chl *a* concentration of 0.77 mg m^{-3} we calculate a production rate of

0.48 mg C m^{-3} h^{-1} at the fluorescence maximum at the seaward station. This rate is low due to light limitation, and it increases the integrated production rate by only 4 %). The productivity indices Λ (integrated production rate divided by the integrated chl *a* concentration) and Ψ (Λ divided by the average irradiance at the sea surface, following Platt 1986) were higher at the landward station by a factor of 1.7 and 1.6 respectively. Differences in the magnitudes of both of these indices are probably significantly underestimated because we underestimated the integrated chl concentration at the seaward station. We calculated a quantum requirement for each euphotic zone ($1/\Phi_e$) by dividing the average I_o values by the integrated production rates (and applying unit conversions). 2801 photons were incident at the sea surface for 1 C atom fixed in the euphotic zone at the seaward station, compared to 1055 photons at the landward station.

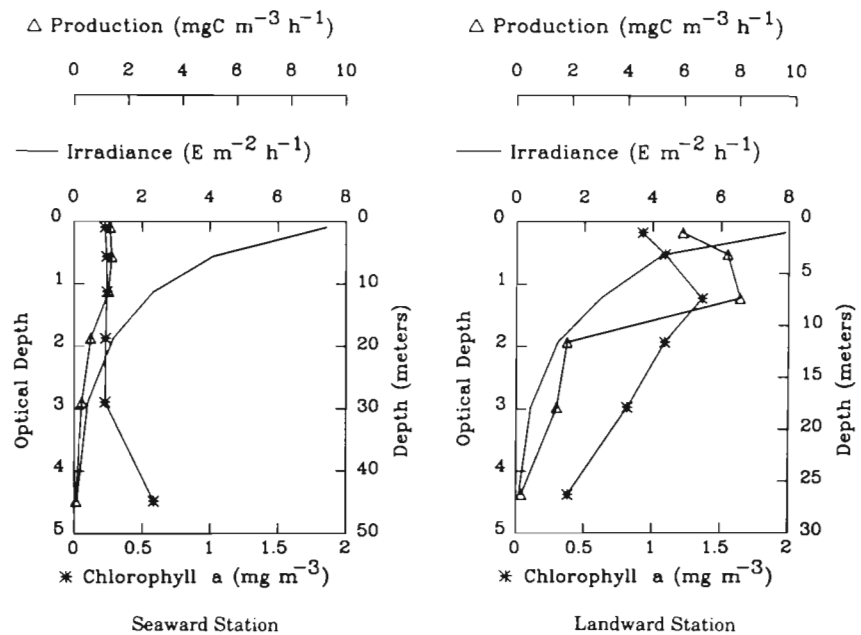
Fig. 4. Vertical profiles of irradiance (estimated from half-day averged values of PAR at the sea surface using secchi-derived extinction coefficients), chl *a* concentration, and production rate scaled to optical depth

Table 1. Comparison of euphotic zone integrations

Term	Description	Units	Seaward station	Landward station
Σchl *a* Δz	Integrated chl *a* concentration	mg chl *a* m^{-2}	14.21	23.37
$\Sigma P\Delta z$	Integrated production rate	mg C m^{-2} h^{-1}	31.83	89.76
Λ	$\Sigma P\Delta z / \Sigma$chl *a* Δz	mg C (mg chl *a*)$^{-1}$ h^{-1}	2.24	3.84
Average I_o	Half day time averaged surface PAR	E m^{-2} h^{-1}	7.43	7.89
K	1.4/secchi depth	m^{-1}	0.09	0.17
Ψ	Λ/Average I_o	mg C (mg chl *a*)$^{-1}$ m^2 E^{-1}	0.30	0.49
$1/\Phi_e$	Average $I_o / \Sigma P\Delta z$	photons carbon^{-1}	2801	1055

Flow cytometer observations

Red fluorescence (relative units) is plotted against particle volume (relative units) for each light depth at the seaward and landward stations in Figs. 5 and 6, respectively. These figures show that there were many more red fluorescing (chl a containing) particles throughout the euphotic zone at the landward station. Ignoring particles with fluorescence values below 7 (these values are not large enough to be distinguished from instrument noise), we see that a single group of relatively small cells (low volumes) was detected at each depth at the seaward station, and its concentration decreased with depth down to 31 m (16 % I_o), and then increased slightly at 48 m (1 % I_o). At the landward station, 2 relatively bright groups of red fluorescing cells (above 30 relative fluorescence units) can be clearly distinguished at depths shallower than 17 m (5 % I_o), and a third smaller and dimmer group is apparent at depths above 11 m (16 % I_o) (see 'Identification of peaks in the flow cytometer data' for a more detailed discussion of these groups).

Species composition (epifluorescence microscopy)

The autotrophic groups enumerated under the epifluorescence microscope at the 30 and 1 % light levels at the seaward and landward stations are listed in Table 2, along with cell size and volume ranges (or averages), cell counts, and total cell volume estimates. These data are summarized in Fig. 7 and Table 3.

The total autotrophic biovolume was by far the largest at 30 % I_o (7 m) at the landward station (Table 3), and *Synechococcus* spp. accounted for about 40 % of it (Fig. 7, Table 3). The cryptomonads, unidentified autotrophs < 10 µm and diatoms also made relatively large contributions to the total biovolume there. At 31 % I_o (12 m) at the seaward station the total autotrophic biovolume was lower by a factor of 5 compared to the landward station, and *Synechococcus* spp. constituted only about 15 % of it (Table 3). The cryptomonads and diatoms did not make large contributions to the autotrophic biovolume there (Fig. 7). Instead, unidentified autotrophs < 10 µm made the largest contribution to the total volume at 31 % I_o at the seaward station, and dinoflagellates and ciliates were the second and third largest groups, respectively (Table 3).

The total autotrophic biovolumes at 1 % I_o at the 2 stations were relatively low (Table 3), and the unidentified autotrophs < 10 µm made the largest contribution at both stations. The *Synechococcus* spp. volume was less than a third of the unidentified autotroph volume in both cases (Fig. 7). The cryptomonads and the diatoms were the second and third largest groups at

1 % I_o at the landward station (Table 3), but the cryptomonads did not make a large volume contribution at 1 % I_o at the seaward station (Fig. 7). Instead, the dinoflagellates made the second largest volume contribution to the total biovolume at 1 % I_o offshore, and the diatoms were the fourth largest group (Table 3).

Identification of the peaks in the flow cytometer data

In Fig. 8 we have superimposed an absolute volume scale (based on bead calibration) on the flow cytometer data from 31 % I_o (7 m) at the landward station, and we
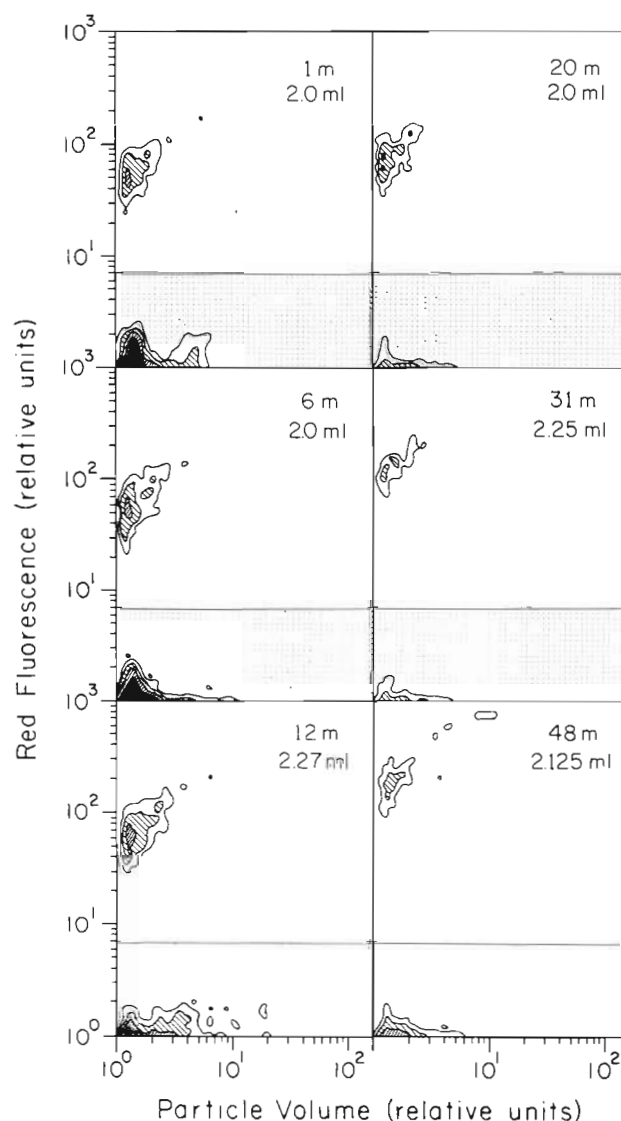

Fig. 5. Contoured scatter plots of particle volume vs red fluorescence (generated with the flow cytometer) for each light depth (100, 58, 31, 16, 5, and 1 % I_o) at the seaward station. Dark shades represent higher frequency of events. Sample depth and volume is shown in the upper right of each panel
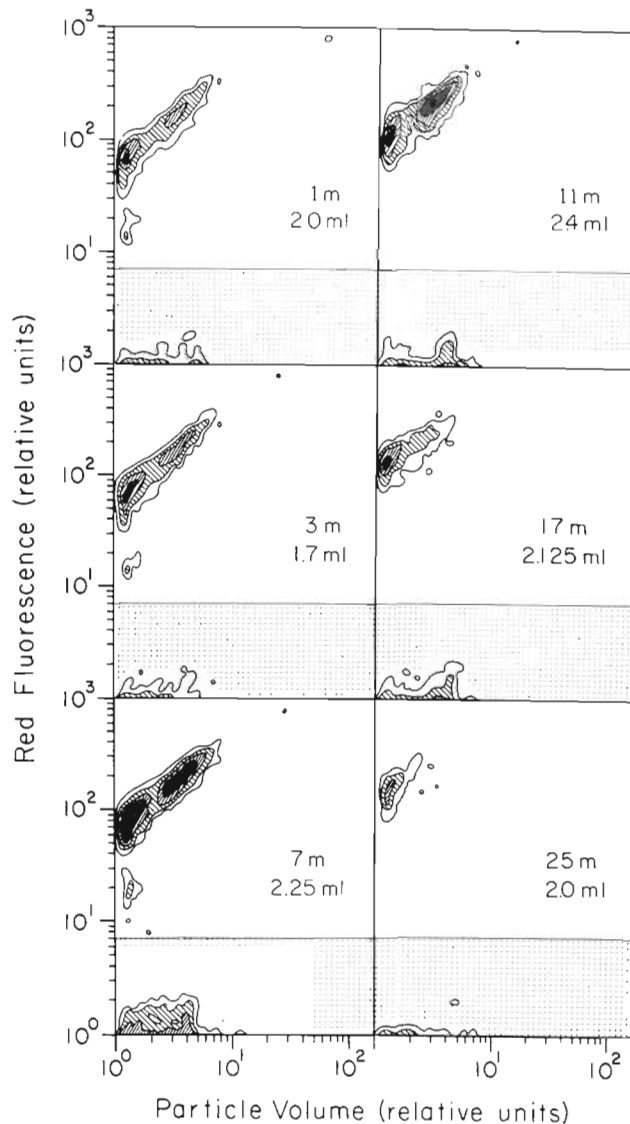
Fig. 6. As in Fig. 5 for the landward station

gated and counted 3 peaks [Group 1 (G_1), Group 2 (G_2) and Group 3 (G_3)] as shown. Since the G_2 and G_3 peaks in Fig. 8 are near the low end of the volume scale (the volume detection limit of the flow cytometer was about 42 μm^3 using a 90 μm aperture), they probably represent partial distributions. That is, it is likely that the smaller cells in these 2 groups passed undetected (note that the G_2 peak appears to be truncated on its left side). Thus, the G_2 and G_3 counts in Fig. 8 are probably underestimates, and we therefore restrict our identification to the G_1 peak.

At 7 m at the landward station (Table 2) the 3 different sized cryptomonad groups are the only epifluorescence microscope counts of the same order of magnitude as the G_1 count in Fig. 8. Since our volume estimate for the largest of the 3 cryptomonad size

classes in Table 2 (7 m) is about the same as the mean volume of the G_1 peak in Fig. 8 ($\approx$ 131 μm^3) we conclude that it represents the larger cryptomonad cells for the most part (the volume estimates for the 2 smaller cryptomonad size classes in Table 2 are below the volume detection limit of the flow cytometer). Thus, Fig. 6 indicates that at the landward station the large cryptomonads were present above the 5 % I_o (17 m) light level, and most abundant at 31 % I_o (7 m). As we pointed out previously, the G_1 peak was absent at the seaward station, suggesting that the large cryptomonads were not present there. However, Table 2 shows that large cryptomonads were in fact present at the seaward station. They were missed by the flow cytometer because their concentration there was lower by almost 2 orders of magnitude, which was below the numerical detection limit of the instrument.

DISCUSSION

Upwelling (extent and source)

Although we occupied our stations near the end of the Oregon upwelling season (Huyer 1977) winds were strong and upwelling favorable for a week prior to sampling. Winds were relaxing as we sampled, but they were still upwelling favorable. The presence of cold water (below 10.0 °C) at the surface along the coast in Fig. 1 and within 10 m of the surface 40 km offshore at the landward station in Fig. 2 confirm active and/or very recent (within days) upwelling (Small & Menzies 1981, Huyer 1983).

Since the density of the water in the euphotic zone at the landward station was generally less than 25.5 kg m^{-3} (Fig. 2), and the deep, permanent pycnocline is defined by densities between 25.5 and 26.0 kg m^{-3} (Huyer 1983), we conclude that the upwelling front between our stations was not where the deep, permanent pycnocline outcropped. Rather, it was where the seasonal pycnocline (summer thermocline) outcropped at the inshore edge of the Columbia River plume (Huyer 1983). Small & Menzies (1981) showed that in late summer under strong steady-state upwelling conditions 2 biomass and productivity cores develop on either side of where the deep, permanent pycnocline outcrops. They speculated that these 2 cores are associated with the 2-celled upwelling circulation proposed by Mooers et al. (1976). If this circulation pattern was present off Oregon during our study, and 2 biomass and productivity cores were associated with them, then our landward station would have been in the seaward cell and biomass core, and the source of the upwelled water would have been from above the deep, permanent pycnocline. Water that is upwelled from above the permanent pycnocline will contain a different phytoplank-

Table 2. Autotrophic groups identified under the epifluorescence microscope at the 30 and 1 % light levels at the seaward and landward stations (note differences in depths), along with cell size and cell volume estimates, cell counts, and total biovolume estimates (see 'Methods' for details)

Autotrophic group	Cell size range or average (length in µm)	Cell volume range or average (µm^3)	Cell count (cells l^{-1})	Total volume (µm^3)
Seaward station, 30 %, 12 m				
Synechococcus spp.	≈ 1.0	0.5	2.18×10^7	1.14×10^7
Unidentified autotrophs	2.0 – 5.0	33.5	8.40×10^5	2.82×10^7
Cryptomonad	5.0 – 10.0	91.6	1.63×10^4	1.49×10^6
Autrophic Gymno- Gyrodinium spp.	≈ 9.0	381.7	1.16×10^4	4.44×10^6
cf. Gonyaulax sp.	≈ 35.0	22 449.3	5.94×10^2	1.33×10^7
Pennate diatom	25.0 – 50.0	1600.0 – 2816.0	2.41×10^3	6.02×10^6
Mixotrophic ciliates	25.0 – 120.0	4090.6 – 113 097.3	9.45×10^2	1.27×10^7
Seaward station, 1 %, 48 m				
Synechococcus spp.	≈ 1.0	0.5	1.92×10^7	1.01×10^7
Unidentified autotrophs	1.5 – 2.5	4.2	3.89×10^6	1.63×10^7
	5.0 – 10.0	220.9	9.43×10^4	2.08×10^7
Cryptomonads	5.0	65.4	8.56×10^3	5.60×10^5
Autrophic Gymno- Gyrodinium spp.	12.0 – 25.0	904.8 – 8181.2	7.41×10^3	9.83×10^6
Unidentified autrophic dinoflagellates	40.0 – 50.0	1675.5 – 3015.9	2.97×10^2	6.31×10^5
Pennate diatoms	7.5 – 120.0	16.9 – 20 000.0	1.10×10^4	2.42×10^6
Rhizosolenia spp.	150.0 – 880.0	2945.0 – 18 095.6	9.90×10^1	1.26×10^6
Centric diatoms	10.0 – 40.0	392.7 – 25 132.7	3.92×10^4	5.26×10^6
Mixotrophic ciliates	30.0 – 40.0	3665.2	$1.58 \ 3 \ 10^3$	5.81×10^6
Landward station, 30 %, 7 m				
Synechococcus spp.	≈ 1.0	0.5	2.91×10^8	1.52×10^8
Unidentified autotrophs	3.0 – 5.0	33.5	2.24×10^6	7.50×10^7
	5.0 – 10.0	220.9	2.10×10^4	4.36×10^6
Cryptomonad	3.0	14.1	7.14×10^5	1.01×10^7
	5.0	23.6	8.27×10^5	1.95×10^7
	10.0	130.9	4.32×10^5	5.66×10^7
Autrophic Gymno- Gyrodinium spp.	≈ 8.0	220.9	2.56×10^4	5.66×10^6
Pennate diatoms	50.0	3200.0 – 7200.0	2.05×10^3	1.18×10^7
Rhizosolenia spp.	500.0 – 840.0	16 493.4 – 39 269.9	1.46×10^3	3.51×10^7
cf. Eucampia	30.0 – 40.0	1131.0 – 9242.8	9.24×10^2	4.87×10^6
Centric diatoms	15.0 – 40.0	1325.4 – 25 132.7	5.65×10^3	1.85×10^7
Chaetoceros spp.	10.0 – 20.0	196.3 – 1570.8	1.39×10^3	7.25×10^5
Mixotrophic ciliates	17.0 – 80.0	1286.2 – 33 510.3	5.76×10^2	3.32×10^6
Myrionecta rubrum	50.0	16 362.5	1.98×10^2	3.24×10^6
Landward station, 1 %, 25 m				
Synechococcus spp.	≈ 1.0	0.5	1.90×10^7	9.95×10^6
Unidentified autotrophs	2.0 – 3.0	8.2	3.22×10^6	2.63×10^7
	5.0 – 10.0	220.9	4.05×10^4	8.94×10^6
Cryptomonads	6.5	54.5	4.43×10^5	2.41×10^7
Autrophic Gymno- Gyrodinium spp.	≈ 10.0	523.6	6.22×10^3	3.26×10^6
Pennate diatoms	10.0 – 50.0	40.0 – 1250.0	2.17×10^4	2.44×10^6
Centric diatoms	25.0 – 100.0	6135.9 – 392 699.1	9.90×10^1	1.40×10^7
Mixotrophic ciliates	40.0 – 80.0	16 755.2 – 134 041.3	6.60×10^1	4.97×10^6

ton seed population and lower nutrient concentrations than water upwelled from below the permanent pycno-cline. This could account for the dominance of Synechococcus spp., cryptomonads, and unidentified auto-trophs (rather than diatoms) at the landward station.

Integrated values and indices

The integrated chlorophyll values in Table 1 are lower than the summertime means for the same locations reported by Small & Menzies (1981), but the

integrated production rate we measured at the landward station (1.15 g C m^{-2} d^{-1} when converted to a daily rate, ignoring nighttime respiration) is comparable to the highest summertime values for the same location reported by Small et al. (1972) (their integrated values varied between about 0.1 and 1.0 g C m^{-2} d^{-1} seasonally over a 4 yr period). The nearshore integrated rate is also slightly higher than the summertime mean for Washington slope waters reported by Perry et al. (1990). We therefore consider that the landward station was relatively productive for northwest coastal waters. However, daily integrated production rates have been measured in coastal upwelling systems that exceed our landward station value by more than a factor of 5 (e.g. off Peru and Baja California; Barber & Smith 1981, Harrison et al. 1981).

Converting the productivity index Λ for the landward station to a daily rate gives 49.53 mg C (mg chl $a)^{-1}$ d^{-1} (again, ignoring nighttime respiration), which is close to the mean of 47 mg C (mg chl $a)^{-1}$ d^{-1} reported by Barber & Smith (1981) for a Peruvian upwelling system. Platt (1986) predicted that Ψ (Λ normalized to insolation) should be relatively constant for different ocean environments, and may be useful for predicting production rate from satellite measurements of chl a. The Ψ values calculated for our seaward and landward stations (Table 1) are near the lower and upper ranges, respectively, of the values reported by Platt (1986). Thus,
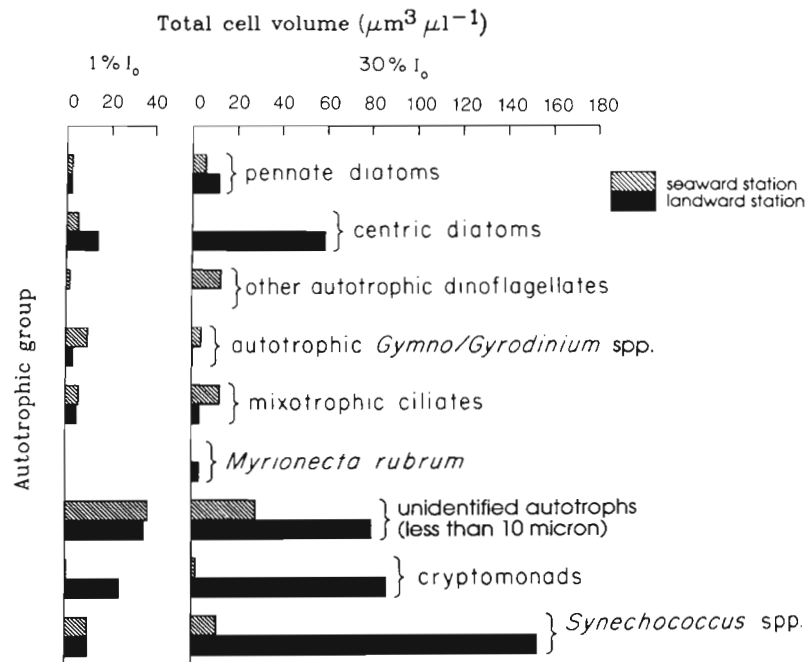

Fig. 7. Comparison of estimated total cell volumes of autotrophic groups identified, measured, and counted under the epifluorescence microscope for the seaward and landward stations at 1 and 30 % light levels. These plots were generated using the data in Table 2. 'Centric diatoms' include all diatoms not identified as pennate, and 'other autotrophic dinoflagellates' include all dinoflagellates not identified as Gymno/Gyrodinium spp.

this index can vary considerably across well-defined oceanographic boundaries.

The $1/\Phi_e$ values that we calculated in Table 1 are similar to the areal energy conversion efficiencies (ε_A) discussed in Kirk (1983). Kirk's ε_A is the ratio of the amount of chemical energy that is photosynthetically stored in the euphotic zone during the ^{14}C incubation period (expressed as energy m^{-2} sea surface) to the

Table 3. The 4 largest autotrophic groups listed in order according to percent of the total biovolume for the 30 and 1 % light depths at both stations

Light depth	Seaward station	Landward station
30 % I_o	Unidentified autotrophs <10 μm (36.4 %) Dinoflagellates[a] (22.9 %) Ciliates[b] (16.4 %) Synechococcus spp. (14.7 %)	Synechococcus spp. (38.4 %) Cryptomonads (21.8 %) Unidentified autotrophs <10 μm (20.1 %) Diatoms[c] (17.9 %)
Total volume:	77.5 μm^3 μl^{-1}	395.9 μm^3 μl^{-1}
1 % I_o	Unidentified autotrophs < 10 μm (50.1 %) Dinoflagellates[a] (15.6 %) Synechococcus spp. (13.6 %) Diatoms[c] (12.1 %)	Unidentified autotrophs < 10 μm (37.4 %) Cryptomonads (25.6 %) Diatoms[c] (17.5 %) Synechococcus spp. (10.5 %)
Total volume:	74.0 μm^3 μl^{-1}	94.0 μm^3 μl^{-1}

[a] All dinoflagellate groups combined
[b] Mixotrophic ciliates and Myrionecta rubrum combined
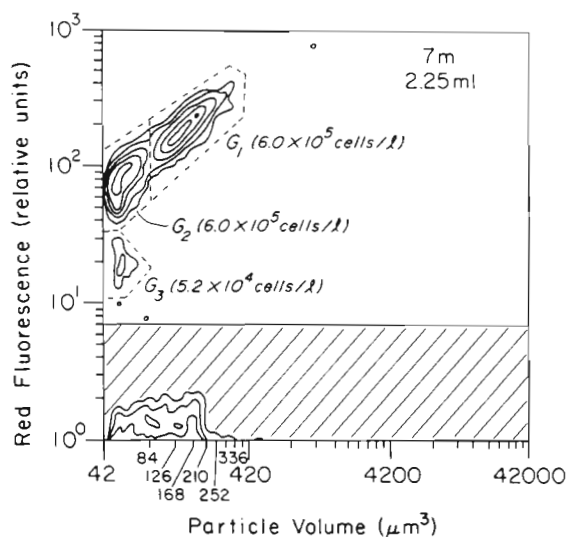[c] All diatom groups combined

Fig. 8. Enlarged, contoured, scatter plot of particle volume vs red fluorescence (generated with the flow cytometer) for the 30 % light depth (7 m) at the landward station. The data were gated as shown to calculate the cell concentrations (G_1: Group 1; G_2: Group 2; G_3: Group 3). A bead calibration was used to determine the absolute volume scale on the horizontal axis

amount of light energy that is available at the sea surface during the incubation period (also expressed as energy m^{-2} sea surface). The result is a dimensionless proportion that expresses the efficiency of photosynthetic utilization of light energy of the entire euphotic zone. We can approximately convert our $1/\Phi_e$ values to ε_A using the relation

$$\varepsilon_A(\%) \simeq 2.171\Phi_e \times 100$$

where 2.171 is the energy required to fix 1 mole of CO_2 divided by the energy content of one mole of photons (PAR) at the sea surface. Using this equation we calculate ε_A values of 0.08 and 0.20 % for the seaward and landward stations, respectively. These values are near the lower and upper ranges of those calculated for moderately productive eastern equatorial Pacific waters (Kirk 1983), but they are low compared to values reported for a eutrophic equatorial upwelling area (ε_A = 0.4 to 1.6 % measured in the Mauritanian upwelling area in the eastern tropical Atlantic; Kirk 1983).

Species composition

Most of the larger autotrophs that we identified under the epifluorescence microscope (e.g *Chaetoceros* spp., *Rhizosolenia* spp., *Myrionecta rubrum* and other pennate and centric diatoms) were not abundant enough to show up as well-defined groups in the flow cytometer data (our numerical detection limit was approximately 10^4 cells l^{-1}). Most were also relatively

unimportant in terms of biovolume (Tables 2 & 3, Fig. 7), and the centric diatoms were the only large-celled group that made a significant contribution at the landward station (Fig. 7). Most of these larger autotrophs can be considered netplankton (that is, they would probably be retained on 20 μm mesh nitex net), and their presence at our landward station is indicative of the upwelling effects. Increases in the netplankton contribution to both primary productivity and standing crop are closely coupled with the occurrence of coastal upwelling, but they typically do not exceed that of the nanoplankton (cells that are not retained on 20 μm mesh nitex net) except during the strongest upwelling pulses (Malone 1971a, b).

Even though *Synechococcus* spp. made a significant contribution to the total autotrophic biovolume at both stations (Tables 2 & 3, Fig. 7) they are not represented in the flow cytometer data because their single-cell volume (approximately 0.5 μm^3) was well below our volume (size) detection limit of 42 μm^3. *Synechococcus* spp. have been recognized as an important component of the autotrophic biomass in oceanic waters for some time (Johnson & Sieburth 1979, Waterbury et al. 1979), but we were surprised to find they represented nearly 40 % of the total biovolume at the 30 % light level at our landward station in the upwelling region (Fig. 7, Table 3). Only a few size fractionation studies of neritic and upwelled waters have shown similarly large contributions to autotrophic biomass by very small cells (those passing either a 1 or 3 μm pore size filters; see results summarized in Booth 1988 and also Chavez 1989).

The unidentified autotrophs < 10 μm were important, in terms of biovolume, on both sides of the front (Tables 2 & 3, Fig. 7). Although we could not positively associate cells in this group with 1 of the peaks in the flow cytometer data, it is likely that they were, in part, responsible for the G_2 peak in Fig. 8. This peak was also present on both sides of the front (Figs. 5 & 6). These unidentified autotrophs were dominated by red-fluorescing flagellates with cell diameters less than 5 μm (Table 2), so most of this biovolume was ultraplanktonic. Several recent studies have indicated that eukaryotic ultraplankton can also be an important component of the total autotrophic biomass of marine systems (e.g. Johnson & Sieburth 1982, Murphy & Haugen 1985, Booth 1988, Chavez et al. 1990).

The cryptomonad biovolume was a large fraction of the total at the landward station in the upwelling region (Tables 2 & 3) and they formed a well-defined group in the flow cytometer data (Figs. 5, 6 & 8). These cells also fall within the ultraplanktonic size range (the largest cryptomonads were about 5 × 10 μm; Table 2). The importance of cryptomonads has probably been overlooked in many taxonomic studies because they are difficult to identify under the light microscope. How-

ever, some studies have indicated that cryptomonads can be an important component of the phytoplankton community in oceanic (Beers et al. 1975, Gieskes & Kraay 1983), and coastal waters (Oslofjord; Throndsen 1978). Using light microscopy, Beers et al. (1971) found that the dominant phytoplankton taxa in 2 patches of upwelled water off Peru were small (2 to 7 μm) flagellates, '... probably cryptomonads or chrysophytes although positive identification was impossible in the Formalin-preserved material'. Cryptomonads are more easily distinguished under the epifluorescence microscope (using 450 to 490 nm excitation) because they contain phycoerythrin and chl *a*, and fluoresce a distinct orange color (e.g. Booth et al. 1982). We were able to detect cryptomonads with the flow cytometer using a combination of chl *a* fluorescence and cell size (volume). Instruments that can also measure phycoerythrin fluorescence should be able to distinguish these cells easily provided that the sample is large enough to detect relatively low cell concentrations (down to at least 10^4 ml^{-1}).

CONCLUSION

The differences in biomass, production rate, and species composition at our 2 stations were clearly related to differences in the physical environment on either side of a sharp thermal front. Upwelling at the landward station supported a higher and more productive autotrophic biomass that was dominated by single-celled species with cell diameters less than 10 μm (e.g. *Synechococcus* spp., cryptomonads and other small autotrophs). *Synechococcus* spp., with cell diameters of about 1 μm, accounted for nearly 40 % of the biomass in the chlorophyll maximum in the upwelling region; large autotrophs, like the centric diatoms, were a relatively minor component. Since small cells were responsible for most of the biomass in the upwelling region we conclude that they were also responsible for the higher integrated production rate and energy conversion efficiency measured there. We believe that the species composition at the landward station was determined by the source of the upwelled water, which apparently came from above the deep, permanent pycnocline along the inshore side of the front. If this type of upwelling is a common occurrence along the frontal region off the Oregon and northern California coasts during the upwelling season, our observations may be indicative of a fairly large scale phenomenon.

LITERATURE CITED

Barber, R. T., Smith, R. L. (1981). Coastal upwelling ecosystems. In: Longhurst, A. R. (ed.) Analysis of marine ecosystems, Academic Press, New York, p. 31–68

Beers, J. R., Reid, F. M. H., Stewart, G. L. (1975). Microplankton of the North Pacific Central Gyre. Population structure and abundance, June 1973. Int. Revue ges. Hydrobiol. 60: 607–638

Beers, J. R., Stevenson, M. R., Eppley, R. W., Brooks, E. R. (1971). Plankton populations and upwelling off the coast of Peru, June 1969. Fish. Bull. U.S. 69: 859–876

Booth, B. C., Lewin, J., Norris, R. E. (1982). Nanoplankton species predominant in the subarctic Pacific. Deep Sea Res. 29: 185–200

Booth, B. C. (1987). The use of autofluorescence for analyzing oceanic phytoplankton communities. Bot. Mar. 30: 101–108

Booth, B. C. (1988). Size classes and major taxonomic groups of phytoplankton at two locations in the subarctic Pacific Ocean in May and August, 1984. Mar. Biol. 97: 275–286

Chavez, F. P. (1989). Size distributions of phytoplankton in the Central and Eastern Tropical Pacific. Global biogeochem. Cycles 3: 27–35

Chavez, F. P., Buck, K. R., Barber, R. T. (1990). Phytoplankton taxa in relation to primary production in the equatorial Pacific. Deep Sea Res. 37: 1733–1752

Curl, H. Jr, Small, L. F. (1965). Variations in photosynthetic assimilation ratios in natural, marine phytoplankton communities. Limnol. Oceanogr. 10: 67–73

Fitzwater, S. E., Knauer, G. A., Martin, J. H. (1982). Metal contamination and its effect on primary production measurements. Limnol. Oceanogr. 27: 544–551

Gieskes, W. W. C., Kraay, G. W. (1983). Dominance of Cryptophyceae during the phytoplankton spring bloom in the central North Sea detected by HPLC analysis of pigments. Mar. Biol. 75: 179–185

Harrison, W. G., Platt, T., Calienes, R., Ochoa, N. (1981). Photosynthetic parameters and primary production of phytoplankton populations off the northern coast of Peru. In: Richards, F. A. (ed.) Coastal upwelling. Coastal and estuarine sciences, Vol. 1. AGU, Washington, D.C., p. 303–311

Huyer, A. (1977). Seasonal variation in temperature, salinity, and density over the continental shelf off Oregon. Limnol. Oceanogr. 22: 442–453

Huyer, A. (1983). Coastal upwelling in the California Current system. Prog. Oceanogr. 12: 259–284

Johnson, P. W., McN. Sieburth, J. (1979). Chroococcoid cyanobacteria in the sea: a ubiquitous and diverse phototrophic biomass. Limnol. Oceanogr. 24: 928–935

Johnson, P. W., McN. Sieburth, J. (1982). In situ morphology and occurrence of eucaryotic phototrophs of bacterial size in the picoplankton of estuarine and oceanic waters. J. Phycol. 18: 318–327

Kirk, J. T O. (1983). Light and photosynthesis in aquatic ecosystems. Cambridge University Press, Cambridge, p. 244–245

Kitchen, J. C., Menzies, D., Pak, H., Zaneveld, J. R. V. (1975). Particle size distributions in a region of coastal upwelling analyzed by characteristic vectors. Limnol. Oceanogr. 20: 775–783

Kitchen, J. C., Zaneveld, J. R. V., Pak, H. (1978). The vertical structure and size distributions of suspended particles off Oregon during the upwelling season. Deep Sea Res. 25: 453–468

Malone, T. C. (1971a). The relative importance of nannoplankton and netplankton as primary producers in tropical

oceanic and neritic phytoplankton communities. Limnol. Oceanogr. 16: 633-639

Malone, T C. (1971b). The relative importance of nanno-plankton and netplankton as primary producers in the California Current system. Fish. Bull. U.S. 69: 799-820

Mooers, C. N. K., Collins, C. A., Smith, R. L. (1976). The dynamic structure of the frontal zone in the coastal upwelling region off Oregon. J. Phys. Oceanogr. 6: 3-21

Murphy, L. S., Haugen, E. M. (1985). The distribution and abundance of phototrophic ultraplankton in the North Atlantic. Limnol. Oceanogr. 30: 47-58

Parsons, T R., Maita, Y., Lalli, C. M. (1984). A manual of chemical and biological methods for seawater analysis. Pergamon, New York

Perry, M. J., Bolger, J. P., English, D. C. (1990). Primary production in Washington coastal waters. In: Landry, M. R., Hickey, B. M. (eds.) Coastal oceanography of Washington and Oregon. Elsevier, New York, p. 117-138

Platt, T. (1986). Primary production of the ocean water column as a function of surface light intensity: algorithms for

remote sensing. Deep Sea Res. 33: 149-163

Ryther, J. H. (1969). Photosynthesis and fish production in the sea. Science 166: 72-76

Small, L. F., Curl, H. Jr, Glooschenko, W. A. (1972). Effects of solar radiation and upwelling on daily primary production off Oregon. J. Fish. Res. Bd Can. 29: 1269-1275

Small, L. F., Menzies, D. W. (1981). Patterns of primary productivity and biomass in a coastal upwelling region. Deep Sea Res. 28: 123-149

Small, L. F., Ramberg, D. A. (1971). Chlorophyll-a, carbon, and nitrogen in particles from a unique coastal environ-ment. Fertility of the Sea 2: 475-492

Throndsen, J. (1978). Productivity and abundance of ultra- and nanoplankton in Oslofjorden. Sarsia 63: 273-284

Venrick, E. L., Hayward, T L. (1984). Determining chloro-phyll on the 1984 CalCOFI surveys. Calif. coop. oceanic Fish. Invest. Rep. XXV: 74-79

Waterbury, J. B., Watson, S. W., Guillard, R. R. L., Brand, L. E. (1979). Widespread occurrence of a unicellular, marine planktonic, cyanobacterium. Nature, Lond. 277: 293-294